Ocean Engineering 165 (2018) 353–364

Contents lists available at ScienceDirect

Ocean Engineering

journal homepage: www.elsevier.com/locate/oceaneng

Numerical modeling and analysis of the dynamic motion response of an offshore wind turbine blade during installation by a jack-up crane vessel

Yuna Zhao[a,c], Zhengshun Cheng[a,b,c,*], Peter Christian Sandvik[d], Zhen Gao[a,b,c], Torgeir Moan[a,b,c], Eric Van Buren[e]

[a] Centre for Autonomous Marine Operations and Systems (AMOS), NTNU, NO-7491, Trondheim, Norway
[b] Centre for Ship and Ocean Structures (CeSOS),NTNU, NO-7491, Trondheim, Norway
[c] Department of Marine Technology, NTNU, NO-7491, Trondheim, Norway
[d] PC Sandvik Marine, Trondheim, Norway
[e] Fred. Olsen Windcarrier, Olso, Norway

ARTICLE INFO

Keywords:
Offshore wind turbine blade installation
Jack-up crane vessel
Soil-structure interaction
Structural flexibility
Fully coupled method
Dynamic motion response

ABSTRACT

Jack-up crane vessels are commonly used to install offshore wind turbine blades and other components. A jack-up crane vessel is subjected to wind and wave loads, which cause motion at crane tip. Excessive motion at crane tip can lead to failure of lifting operations. Therefore, the crane tip motion should be properly assessed for jack-up crane vessels. In this study, a fully coupled model is developed for a typical elevated jack-up crane vessel, considering the hydrodynamic and aerodynamic loads on the vessel, the soil-structure interaction, and the structural flexibility of the jack-up legs and crane. The vessel model developed is further coupled with the SIMO-Aero code to achieve a fully coupled aero-hydro-soil-elastic-mechanical code SIMO-RIFLEX-Aero for numerical modeling and dynamic analysis of offshore single blade installation using jack-up crane vessels. The SIMO-RIFLEX-Aero code is then applied to study the dynamic response of the DTU 10 MW wind turbine blade installed by a typical jack-up crane vessel under various wind and wave conditions. The results show that significant motion is induced at crane tip, mainly due to wave loads. It is important to consider the structural flexibility of the jack-up legs and crane when modeling the installation of offshore wind turbine blades.

1. Introduction

Offshore wind turbines can be installed by either floating or jack-up crane vessels, as shown in Fig. 1. Compared to jack-up vessels, floating vessels provide more flexibility for offshore operations and accessibility in deep water. They have been used to install fully assembled wind turbine towers with rotors and nacelle for floating and jacket-supported offshore wind turbines, as presented in Fig. 1(a) and (b). However, such operations are very challenging and rarely used due to the wave-induced motion of the floating crane vessels.

Jack-up crane vessels are commonly used to install offshore wind turbines in shallow water, because they can provide a stable working platform. They are able to install the components of offshore wind turbines (such as foundation, tower, nacelle and blades) separately and in sequence, as shown in Fig. 1(c) (Ahn et al., 2017). Due to the growing market for offshore wind energy, the demand for use of jack-up crane vessels keeps increasing (Global Data, 2014).

Compared to traditional jack-up platforms used in the offshore oil and gas industry, the jack-up crane vessels for offshore wind turbine installation usually have shallower leg penetration into the seabed because of the frequent repositioning. As a result, the vessels are more sensitive to wind and wave loads. The tip of the crane on the vessel is observed to have notable motion during offshore operations. Large crane tip motion can lead to damaged guide pins at blade root during the blade installation. To ensure safe and cost efficient operations, it is of great importance to study the dynamic response of the jack-up crane vessel, especially of the crane tip and the installed components.

To date, limited work has been carried out on jack-up crane vessels used in offshore wind turbine installation. Duan and Olsson (2014) and Ringsberg et al. (2017) studied the soil impact loads on the spudcans of a jack-up crane vessel during the lowering and retrieval phases of jack-up legs. Weather window assessments were also conducted based on the spudcan impact force criteria. It was found that the leg lowering and retrieval operations are possible under larger wave heights in long waves. Van Dalfsen (2016) studied the effects of soil load modeling on the dynamic structural response of the jack-up crane vessel under

* Corresponding author. Department of Marine Technology, NTNU, Otto Nielsens Vei 10, NO-7491, Trondheim, Norway.
E-mail addresses: yuna.zhao@ntnu.no (Y. Zhao), zhengshun.cheng@ntnu.no (Z. Cheng).

https://doi.org/10.1016/j.oceaneng.2018.07.049
Received 12 March 2018; Received in revised form 12 June 2018; Accepted 15 July 2018

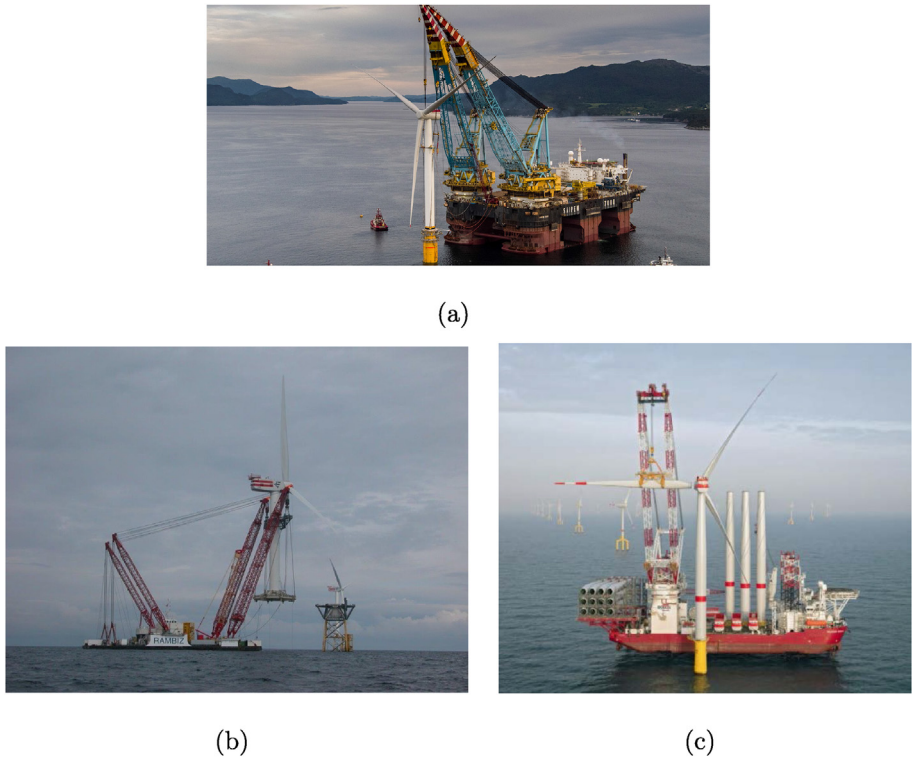

Fig. 1. Installation of offshore wind turbines: (a) and (b) Installation of fully assembled tower by floating crane vessels (Carbon Brief Ltd, 2017; Scaldis Salvage & Marine Contractors NV, 2018); (c) Single blade installation for using a vessel (Fred. Olsen Windcarrier AS, 2017).

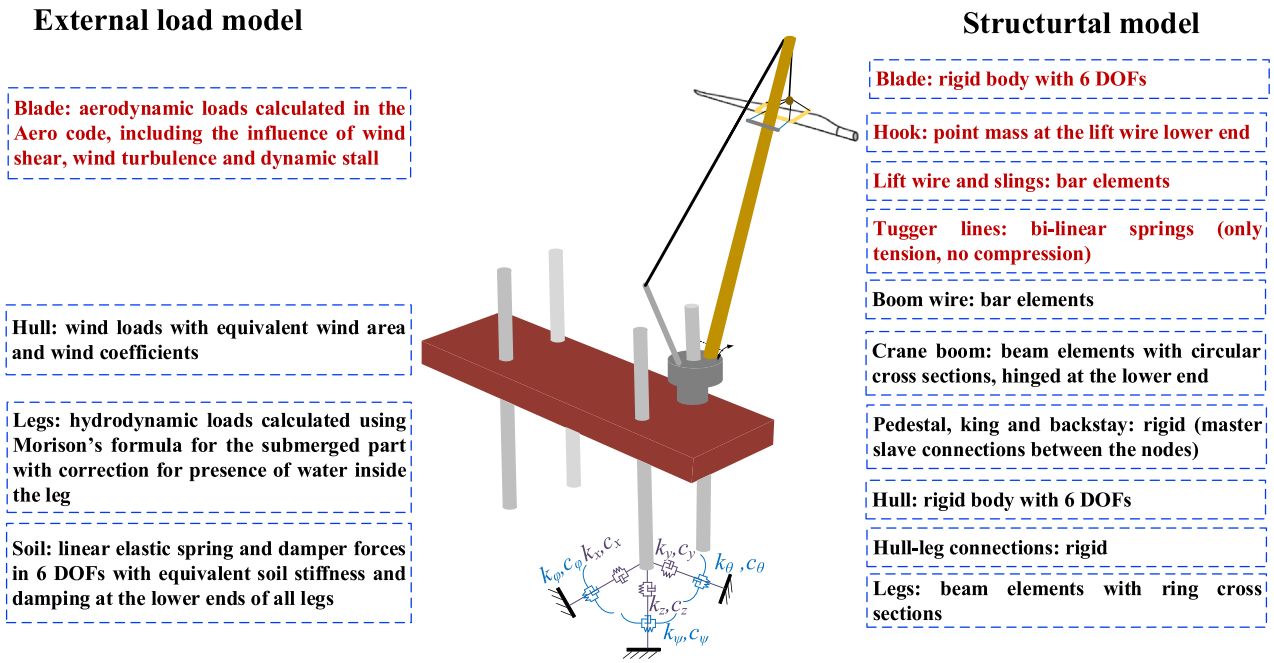

Fig. 2. The structural and external force models of a typical elevated jack-up crane vessel. The blade and the lifting gear are also illustrated here to give an overview of the fully coupled aero-hydro-soil-elastic-mechanical code, i.e., SIMO-RIFELX-Aero, for simulating installation of offshore wind turbine blades by jack-up crane vessels. The integration of the codes and the modeling of the blade and the lifting gear are discussed in details in Section 5.

survival conditions. The results indicated that advanced soil models are essential in the design check of jack-up crane vessels in extreme sea states. However, the dynamic motion response of the vessels during crane operations are not considered in these studies.

Zhao et al. (2018) developed an integrated dynamic analysis method for simulating installation of a single blade for wind turbines. The coupled aero-hydro-mechanical code SIMO-Aero was developed and verified, which is capable of accounting for blade aerodynamics, vessel hydrodynamics and system mechanical couplings. The SIMO-Aero code was used to study the dynamic response of a single blade installed by a jack-up crane vessel; however, the motions of the vessel and the crane were not considered by Zhao et al. (2018).

In the present study, a fully coupled model is developed for a typical jack-up crane vessel by using the SIMO (SINTEF Ocean, 2017b) and

RIFLEX (SINTEF Ocean, 2017a) codes. The SIMO and RIFLEX codes were developed by SINTEF Ocean and have been widely used in the offshore wind, oil and gas industries. The vessel model can account for the wave loads on the jack-up legs, the wind loads on the vessel, the structural flexibility of the vessel legs and the on-board crane, and the soil-structure interaction. Eigen value analysis is conducted to identify the eigen periods and mode shapes of the vessel. The first two longest natural periods are compared against values calculated according to standard recommended formula to evaluate the numerical model. Then the vessel model developed is integrated with the SIMO-Aero code developed by Zhao et al. (2018) to achieve a fully coupled aero-hydro-soil-elastic-mechanical code, i.e., SIMO-RIFLEX-Aero, for offshore wind turbine blade installation by a jack-up crane vessel. Afterwards, a series of time domain simulations are carried out to study the dynamic response characteristics of the vessel, the cane tip and the installed blade under different wind and wave conditions. The effects of crane tip motion on the dynamic response of the installed blade are also investigated.

2. Numerical modeling of the elevated jack-up crane vessel

In this section, a coupled model is developed for typical elevated jack-up crane vessels based on the SIMO-RIFLEX code, as shown in Fig. 2. The vessel model accounts for the structural flexibility of the legs and the crane, the soil-spudcan interaction, the wave loads on the legs and the wind loads acting on the vessel. The vessel model developed is later integrated with the SIMO-Aero code in Section 5 to formulate the SIMO-RIFLEX-Aero code, a fully aero-hydro-soil-elastic-mechanical coupled code, for simulating offshore wind turbine blade installed by jack-up crane vessels.

The hull of the vessel is modeled as a rigid body with 6 degrees of freedom (DOFs) in SIMO, because it is generally much stiffer in all directions, compared to the jack-up legs and the crane. The jack-up legs are modeled by use of flexible beam elements in RIFLEX. The spudcans are modeled as nodal bodies at the lower end of each leg.

The jack-up legs are connected to the hull by jacking systems installed in the white jacking houses shown in Fig. 3(a). Fig. 3(b) shows the rock-chock type jacking system which is commonly used in modern jack-up vessels. It forms very stiff clamped connections between the legs and the hull. The flexibility of such jacking system has negligible influence on the system natural periods (Global Maritime, 2003). Thus, the hull-leg connections are modeled as rigid connections in the present model.

Pedestal crane is a typical type of cranes equipped on jack-up crane vessels. As shown in Fig. 4(a), a pedestal crane consists of crane supports, a wire overhang system and a lattice boom. In the numerical model, it is assumed that the deformation of the crane system are mainly due to the flexibility of the boom and boom wires. The deformation of the crane supports, including king, pedestal and back-stay, is neglected. The lattice boom is simplified into a circular RIFLEX beam with equivalent structural stiffness properties. The lower end of the boom is hinged on the crane base. The boom inclination is controlled by the boom wires which are modeled as RIFLEX bar elements.

2.1. Modeling of soil-spudcan interaction

In the present model, the soil reaction force is represented by using equivalent linear elastic springs combined with linear dampers to consider the soil damping effects, without detailed modeling of the spudcans, as shown in Fig. 5. It is a feasible simplification for modeling of soil behavior for jack-up crane vessels under operational sea states which typically have a significant wave height below 2.5–3.0m (Ahn et al., 2017; Paterson et al., 2017). In such conditions, the loads acting on the spudcans are much smaller than those required to reach the soil yield surface. Hence, the linear elastic soil modes can be used (Martin, 1994; Zeng et al., 2015).

As shown in Fig. 5, linear springs and dampers in 6 DOFs at the reference point are used to represent the soil resistant force. The reference point of the soil model is at the lower end of each jack-up leg where the spudcan locates. The corresponding soil reaction force can be expressed as a function of spudcan displacement, i.e.:

$$\mathbf{F}_s = \mathbf{K}_s\mathbf{X}_{sc} + \mathbf{C}_s\dot{\mathbf{X}}_{sc} \tag{1}$$

where the dots denote time derivative; $\mathbf{K}_s = [k_x \quad k_y \quad k_z \quad k_\phi \quad k_\theta \quad k_\psi]$ is the soil stiffness vector in 6 DOFs without considering coupling effects. The stiffness coefficient are dependent on the soil properties, the dimension and the penetration depth of the spudcans. They could be calculated using recommended empirical formula (SNAME, 2008; ISO, 2009) or estimated based on site-specific soil properties. The $\mathbf{C}_s$ is the corresponding vector of the soil damping. $\mathbf{X}_{sc}$ is the displacement vector, i.e.:

$$\mathbf{X}_{sc} = [x \quad y \quad z \quad \phi \quad \theta \quad \psi] \tag{2}$$

where x, y, z are the translation motion of the reference point (lower end node of jack-up leg); ϕ, θ and ψ are the rotational motion of the leg at its lower end.

2.2. Modeling of the wave loads

A jack-up crane vessel usually has its hull elevated well above the mean sea surface when installing offshore wind turbines. Only the lower parts of the legs are submerged. As shown in Fig. 6, the instantaneous wave load normal to the leg can be calculated using Morison's formula (leg diameter to wave length ratio < 1/5):

Fig. 3. Hull-leg connections for typical offshore jack-up crane vessels: (a) Jacking houses (A2SEA, 2017); (b) Rack-chock type jacking system (Friede and Goldman Ltd, 2017).

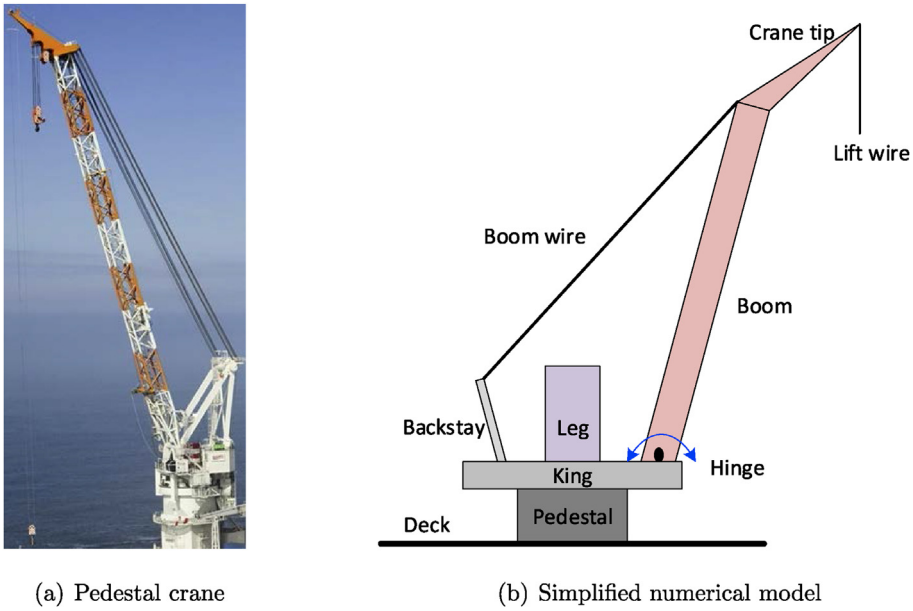

Fig. 4. Illustration of a typical offshore pedestal crane and its numerical model.

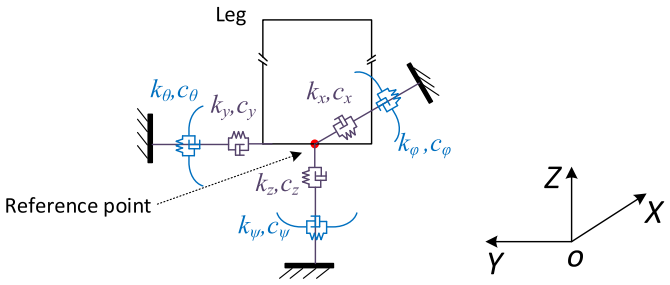

Fig. 5. Modeling of soil resistance force on the spudcan using linear springs and dampers.

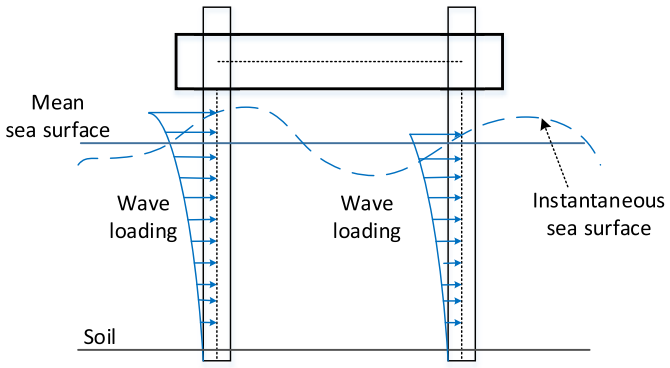

Fig. 6. Wave loads on jack-up legs.

$$\mathbf{F} = \int_{-h}^{\eta} \left[\rho A_{ext}(1 + C_A)\dot{\mathbf{u}}(z) - \rho A_{ext} C_A \ddot{\mathbf{r}}(z) + \frac{1}{2}\rho D_{ext} C_D |\mathbf{u}(z) - \dot{\mathbf{r}}(z)|(\mathbf{u}(z) - \dot{\mathbf{r}}(z)) - \rho A_{int} \ddot{\mathbf{r}}(z) \right] dz \tag{3}$$

where the dots denote time derivatives; ρ is the mass density of water; D_{ext} is the external diameter of the leg; A_{ext} and A_{int} are respectively the external and internal cross-sectional areas of the leg; C_A and C_D are respectively the non-dimensional 2D added mass and quadratic drag coefficients; **u** and **r** are respectively the velocity vector of undisturbed wave field and motion vector of the leg; h is the water depth and η is the instantaneous wave elevation. The last term in Eq. (3) represents the effect of water inside leg (SINTEF Ocean, 2017a).

2.3. Modeling of the wind loads

During offshore wind turbine installation, the wind loads on the jack-up crane vessel consists of contributions from the jack-up house, legs, as well as the wind turbine components and equipment loaded on the vessel deck. The wind area and shape coefficients of each component are different. The wind load on one component may be greatly affected by shielding effect from others. Detailed coefficients from wind tunnel test are favorable in order to achieve an accurate estimation of wind loads. However, these coefficients are not available at present. Under such a circumstance, the wind area above the hull baseline is considered as a block with equivalent area and wind coefficients. The wind loads on the parts of the legs between the wave crest and the hull baseline are neglected as recommended (DNVGL, 2015). The simplification is acceptable since the motion of the jack-up vessel is mainly wave-induced during operations. The wind load is calculated as (DNVGL, 2015):

$$F_{x,wd} = \frac{1}{2}\rho_{air} C_S A V^2 \cos\alpha \tag{4}$$

$$F_{y,wd} = \frac{1}{2}\rho_{air} C_S A V^2 \sin\alpha \tag{5}$$

$$F_{z,wind} = 0 \tag{6}$$

where ρ_{air} is the density of air; α is the relative wind inflow angle, as shown in Fig. 7; V is the relative wind inflow velocity; C_S is the overall shape coefficient, i.e., $C_S = 1.1$; A is the area normal to the inflow wind:

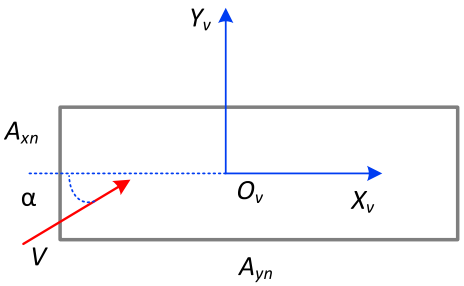

Fig. 7. Illustration of wind area and relative wind inflow angle (top view).

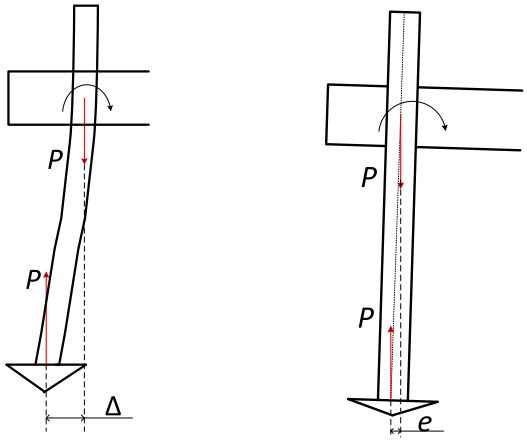

(a) P-Δ effect (b) Leg inclination

Fig. 8. Illustration of P-Δ effect and leg inclination.

$$A = A_{xn}|cos\alpha| + A_{yn}|sin\alpha| \tag{7}$$

where A_{xn} and A_{yn} are respectively the wind area normal to X_v and Y_v axis. The corresponding wind moments can be expressed as:

$$M_{x,wd} = -z_c F_{y,wd} \tag{8}$$

$$M_{y,wd} = z_c F_{x,wd} \tag{9}$$

$$M_{z,wd} = x_c F_{y,wd} - y_c F_{x,wd} \tag{10}$$

where $[x_c \quad y_c \quad z_c]$ is the position vector of the center of the equivalent wind block.

2.4. Modeling of $P-\Delta$ effect and influence of leg inclination

For slender and flexible jack-up structures, the second order effects need to be considered, such as the $P-\Delta$ effect and the influence of leg inclination (SNAME, 2008).

The $P-\Delta$ effect is illustrated in Fig. 8(a). The deformation of jack-up legs causes hull translational motion in the horizontal plane. As a result, the vertical soil reaction force no longer passes through the center of hull-leg connection and leads to an extra moment. Inclination of the legs, as illustrated in Fig. 8(b), results in an eccentricity between the vertical soil force and the hull-leg connection. It also introduces extra bending moment in the legs at the hull-leg connections. These two effects are accounted for by the non-linear geometry feature in the finite element model in RIFLEX.

2.5. Modeling of system damping

For a typical jack-up type structure, the damping sources are mainly structural damping, soil damping and hydrodynamic damping.

The hydrodynamic damping is accounted for by incorporating the wave velocity relative to the movement of legs, which is the third term in Eq. (3).

The soil damping is typically around 2% of the system critical damping (DNVGL, 2015). In this study, the soil damping is considered by using equivalent linear dampers, which are presented as the second term in Eq. (1).

The structural damping of jack-up crane vessels also includes damping in guides, shock pads, locking devices and jacking mechanisms. In the present model, the structural damping corresponds to 0.5% of the system critical damping and is modeled by use of the Rayleigh damping model (Rayleigh, 1877).

Table 1
Main properties of the vessel (Fred. Olsen Windcarrier AS, 2016).

Parameter	Value
Hull length, breadth and depth [m]	132, 39, 9
Total elevated load [t]	16,900
Total wind area A_{xn}, A_{yn} [m^2]	5372, 2119
Center of wind area (x_c, y_c, z_c) [m]	(0, 0, 7.5)
Leg length [m]	92.4
Leg diameter [m]	4.5
Longitudinal leg spacing [m]	68.3
Transverse leg spacing [m]	30.6

Table 2
Main parameters of the crane.

Parameter	Value
Height of crane base [m]	25.5
Boom length [m]	107.6
Crane boom angle[deg]	67.6
No. of equivalent boom wires [-]	2
Equivalent boom wire stiffness [kN/m]	9048
Equivalent boom wire damping [kNs/m]	90.5

3. System description of a typical jack-up crane vessel

A typical jack-up crane vessel is used in this study. The main properties of the vessel are listed in Table 1, including the parameters of the hull, legs and wind coefficients.

The structural properties of the crane are presented in Table 2. The detailed site-specific data for the vessel and the corresponding soil parameters are given in Table 3, which were obtained when the vessel installed offshore wind turbines at a 39m-deep site in the North Sea.

3.1. Definition of coordinate systems

A global coordinate system and a vessel-related coordinate system are introduced, as shown in Fig. 9.

For the vessel-related coordinate system $O_v - X_v Y_v Z_v$, the origin O_v is located at the hull geometry center with X_v−axis along the hull length and Y_v−axis along the hull width while the z_v−axis follows the right hand rule.

The global coordinate system $O-XYZ$ has its origin located at the mean sea surface. The X and Z respectively parallel with Y_v and Z_v, when the vessel is at rest.

The crane boom angle is defined as the relative angle between the crane boom and the deck. The wave incident angle θ_{wv} is defined as the angle of the wave direction relative to the X and is positive

Table 3
Site specific data of the vessel.

Parameter	Value
Water depth [m]	39.1
Airgap [m]	7.2
Penetration [m]	2.7
Leg below hull [m]	49
C_A (2D added mass coeff.)	1.0
C_D (2D drag coeff.)	0.8
Soil type	Dense sand
K_x, K_y [kN/m]	1.35×10^6
K_z [kN/m]	1.47×10^6
K_ϕ, K_θ [kNm/deg]	6.4×10^5
K_ψ [kNm/deg]	8.3×10^5

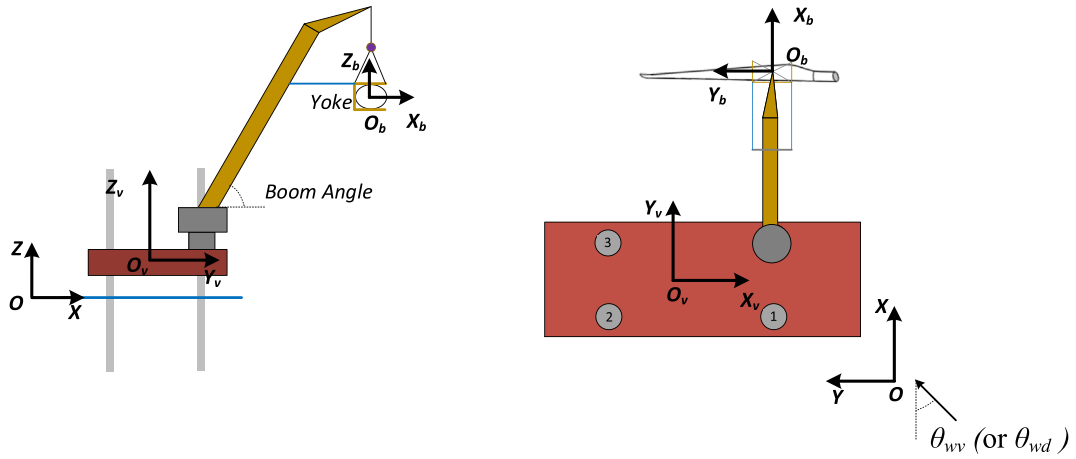

(a) Side view (b) Top view

Fig. 9. Definition of the global coordinate system $O-XYZ$ and the vessel-related coordinate system $O_v - X_vY_vZ_v$. A blade is also presented here to illustrate the scenario of wind turbine blade installation discussed in detail in Section 5. The wind turbine blade is along the y_g axis. A blade-related coordinate system $O_b - X_bY_bZ_b$ is defined for the blade; its origin is located at the blade COG and it is parallel with the global coordinate system when the blade is at rest.

counterclockwise. A similar definition is used for the wind inflow angle θ_{wd}.

The vessel is used to install a wind turbine blade, as shown in Fig. 9. Detailed modeling of the blade and the lifting gear is discussed in Section 5.

3.2. Cancellation and enhancement periods of wave loads on the legs

Table 4 gives the critical wave periods that could lead to cancellation and enhancement effects of the global wave loads on the vessel legs due to wave phase, caused by the spacing between legs (DNVGL, 2015).

The wave loads on individual legs are not affected. The resulting total loads on all of the legs would be reduced to zero due to the opposite phases of wave loads on the two legs in the wave propagation direction when the cancellation effect happens. Otherwise, the sum wave loads would be doubled in case of same phases, which is the enhancement effect of wave loads. Some of these cancellation and enhancement periods are likely to occur when the vessel works in the North sea (typical wave period 5~15s). The influences of wave cancellation and wave enhancement effects on the system dynamic response are studied in the later sections.

4. Evaluation of the vessel numerical model

The developed vessel model is evaluated in this section. The natural periods of the vessel motion obtained from the numerical model are compared against values estimated according to standard-recommended empirical formula. Verification against experimental data or on-site measurement is not carried out since these data are very difficult to obtain.

Eigen-value analysis is conducted to identify the eigen periods and eigen modes of vessel motion (excluding the crane), which are presented in Table 5 and Fig. 10. The first two largest natural periods correspond to surge and sway motion, followed by that of yaw motion, which agrees with the general order of natural periods for typical elevated jack-up vessels given in DNV-RP-C104 (DNVGL, 2015).

Table 4
Cancellation and enhancement periods for the global wave loads on the vessel legs.

Direction	0^o	65.87^o	90^o
T_{cancel}[s]	6.26 3.61	10.17 5.65	9.61 5.40
$T_{enhance}$ [s]	4.43 3.13	6.93 4.90	6.62 4.68

Table 5
Eigen periods of the vessel motion defined in the vessel-related coordinate system in Fig. 9.

Mode	1	2	3	4	5	6
Eigen period (s)	3.087	2.912	2.363	0.594	0.479	0.451
Dominant hull motion	Sway	Surge	Yaw	Roll	Pitch	Heave

According to DNV-RP-C104 (DNVGL, 2015), the longest natural periods of a typical elevated unit can be approximated by:

$$T_n = 2\pi\sqrt{\frac{m_e}{k_e}} \tag{11}$$

where m_e and k_e are respectively the equivalent mass and stiffness associated with one leg, which have to be obtained from the complete model of the jack-up vessel and four legs, depending on the eigen modes. The natural periods of surge and sway motion for the vessel are calculated by using Eq. (11) and compared with the corresponding values obtained from the eigen-value analysis, as given in Table 6. The comparison shows that the eigen-periods of the eigen-value analysis agree fairly well with those estimated by the empirical formula. It implies that the established numerical model can provide reasonable estimation of the vessel dynamic response.

The natural period of the crane motion is identified by using decay tests while the vessel is fixed. A vertical force is applied at the crane tip and removed after some time. The natural period of the crane is calculated by analyzing the time series of the crane tip motion. The natural period is caused by the rotational motion of the crane boom around its hinged lower end due to the boom wire deformation. The crane boom itself has marginal deformation, compared to that of the boom wires. The natural period of the crane is affected by the lifted components and lifting gears. The crane itself has a natural period of 2.0s without lifting anything. However, when the installed blade and the lifting gear given in Section 5 are considered, the crane natural period is shifted to approximately 2.9s.

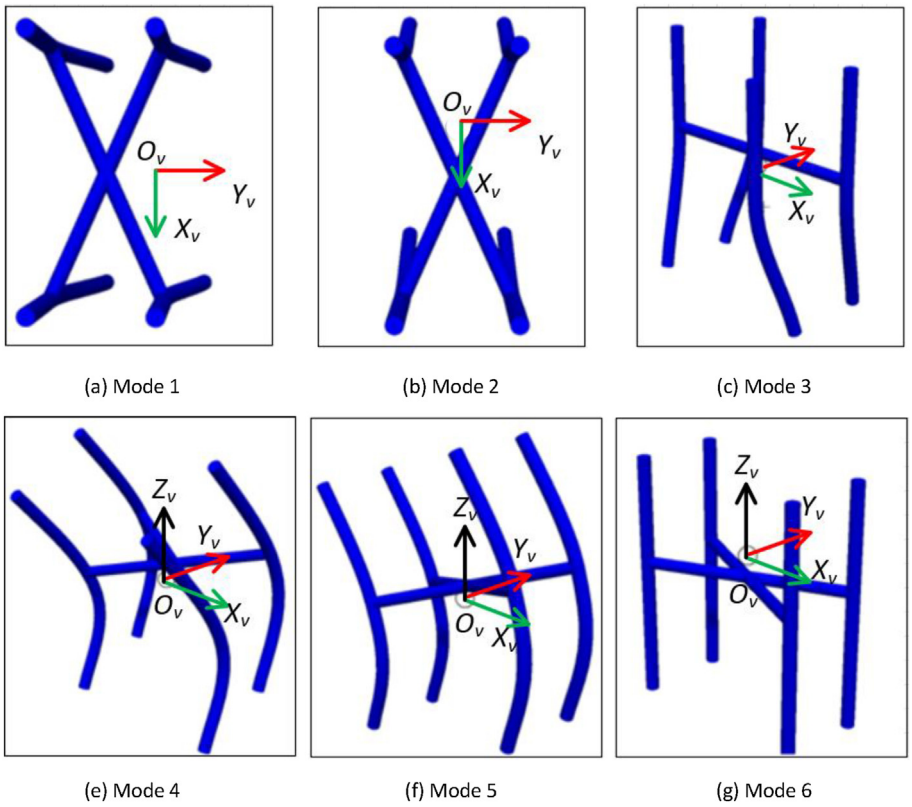

Fig. 10. Illustration of mode shapes of the vessel motion (amplified by 2000 times). The vessel hull is illustrated by two rigid crossing beams. The crane and blade are not considered in the eigen value analysis while the soil-spudcan interaction is included.

Table 6
Comparison of the natural periods of the vessel surge and sway motion (defined in the vessel-related coordinate system in Fig. 9) from eigen value analyses and empirical formula.

Mode	1	2
Dominant hull motion	Sway	Surge
Natural period from eigen value analysis (s)	3.087	2.912
Natural period calculated by Eq. (11) (s)	3.256	3.053

5. Modeling of the installed wind turbine blade and the lifting gear

The developed vessel model is coupled with the SIMO-Aero code developed by Zhao et al. (2018) to establish a fully coupled aero-hydro-soil-elastic-mechanical code, SIMO-RIFLEX-Aero, for simulating offshore wind turbine blade installation using jack-up crane vessels. The coupled code is capable of accounting for the aerodynamics of the installed blade, the structural flexibility of the vessel legs and crane, the wave loads on the legs and wind loads on the hull, the soil-structure interaction, as well as the mechanical couplings between the crane and the blade. The vessel model is extensively discussed in Section 2. The detailed model of the blade and corresponding lifting gear is explained in this section.

The blade is modeled as a rigid body with 6 DOFs in SIMO. The structural flexibility of the blade is neglected since it has minor influence on the dynamic motion response of the blade during installation (Zhao et al., 2018). The aerodynamic loads acting on the blade are calculated by the external code Aero based on the cross-flow principle. Details of the Aero code can be found in Ref. (Zhao et al., 2018). The DTU 10 MW wind turbine blade (Bak et al., 2013) is considered in the present study.

A yoke is used to hold the blade. The yoke and the blade are considered as one rigid body in the numerical model. The yoke is lifted by the hook via four slings. The lift wire runs through the crane tip to the hook. In the present model, the lift wire and slings are modeled as bar elements with equivalent stiffness and damping properties. The hook is modeled as a point mass at the lower end of the lift wire. Tugger lines are used for blade heading control which run from the yoke to a trolley on the crane boom. Pretension is applied in tugger lines to prevent slack lines. The tugger line tension is modeled as bi-linear spring force (Zhao et al., 2018). The main properties of the blade lifting system are summarized in Table 7.

Installation of the DTU 10 MW wind turbine blade by the aforementioned jack-up crane vessel will be simulated by the coupled code SIMO-RIFLEX-Aero. As shown in Fig. 11, the blade span is deployed along the vessel longitudinal direction. A blade body-related coordinate system is defined and used in the presented study. The its origin is at the blade center of gravity. The Y_b−axis is along the blade span. The X_b−axis goes from the leading edge to the trailing edge of the blade while the Z_b−axis follows the right hand rule. The blade body-related coordinate parallels with the global coordinate when the blade is at rest, as shown in Fig. 9.

Table 8 lists the first three longest natural periods and

Table 7
Main properties of the blade and the lifting gear.

Parameter	Value
Hook mass [tons]	10
Yoke mass [tons]	47
Blade mass [tons]	41.67
Blade length [m]	86.37
Installation height [m]	119
Tugger line arm length (relative to blade COG) [m]	10
Length of crane wire (from crane tip to hook) [m]	4.7
Length of slings [m]	20.4

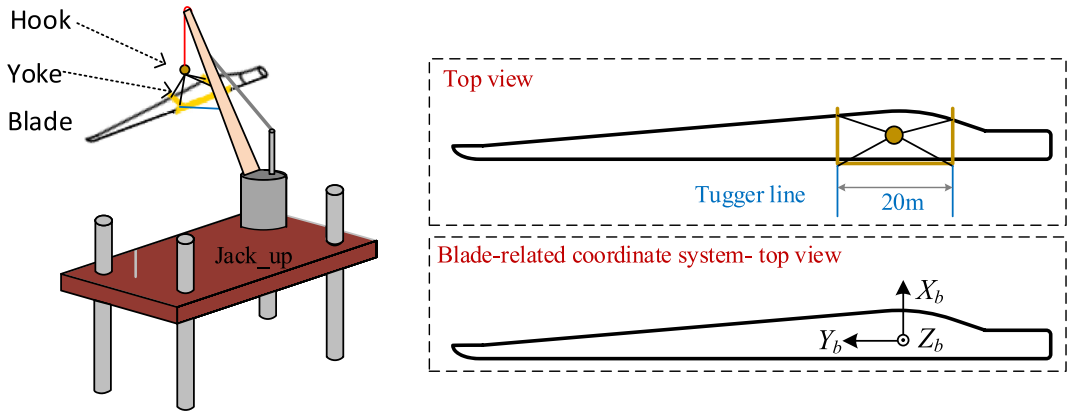

Fig. 11. Illustration of blade orientation and its body-related coordinate system. Definition of the blade motion at its COG: the translational (rotational) motion along the X_b-, Y_b- and Z_b-axis are respectively denoted as surge (roll), sway (pitch) and heave (yaw).

Table 8
Natural periods and corresponding dominant motions of the blade motion response(only blade).

Mode	T_n [s]	ω_n [rad/s]	Dominant response
1	12.0	0.524	Blade roll resonance (blade pendulum around the hook)
2	5.11	1.23	Blade yaw resonance
3	3.63	1.73	Blade-hook double pendulum around the crane tip in the $O_bY_bZ_b$ plane (blade and hook motion out of phase)

corresponding motion which dominate the blade rigid body motion (obtained when the crane tip is fixed). The first mode is caused by the blade pendulum motion around the hook, which is denoted by the blade roll resonant response in this study. The blade yaw resonant motion dominate the second mode. The third mode is caused by the double pendulum motion of the blade and hook around the crane tip in the vertical $O_bY_bZ_b$ plane with the blade and hook motion out of phase (Zhao et al., 2018).

6. Time domain simulations and case studies

Time domain simulations are carried out to study the dynamic response of the vessel and the installed blade under different sea states, using the fully coupled SIMO-RIFLEX-Aero code. A series of load cases are defined, as given in Table 9.

Table 9
Load cases used in the time domain simulations.

	Crane tip	Turbulent wind			Irregular waves		
		U_W [m/s]	T_I [%]	θ_{wd} [deg]	H_s [m]	T_p [s]	θ_{wv} [deg]
LC1	Fixed	10.23	20.8	0	–	–	–
LC2	Free	10.23	20.8	0	–	–	–
LC3	Free	10.23	20.8	0	2.4	8.55	0
LC4	Free	10.23	20.8	30	2.4	8.55	30
LC5	Free	10.23	20.8	65.87	2.4	8.55	65.87
LC6	Free	10.23	20.8	0	2.4	8.55	65.87
LC7	Free	10.23	20.8	0	2.4	8.55	90
LC8	Free	10.23	20.8	0	1.8	8.55	65.87
LC9	Free	10.23	20.8	0	1.2	8.55	65.87
LC10	Free	10.23	20.8	0	2.4	6.93	65.87
LC11	Free	10.23	20.8	0	2.4	5.65	65.87
LC12	Free	7.02	24.8	0	2.4	8.55	65.87
LC13	Free	4.86	30.4	0	2.4	8.55	65.87

U_W- mean wind speed; T_I- turbulent wind intensity; θ_{wd}- wind direction; H_s- significant wave height; T_p- wave peak period; θ_{wv}- wave direction.

LC1 and LC2 are turbulent wind only cases. The vessel and the crane tip are assumed to be fixed in LC1 and are free to move in LC2. These two cases are used to evaluate the wind induced motion of the vessel and the crane tip. Moreover, comparing results of LC1 and other cases can identify the effect of crane tip motion on the motion of the installed blade.

LC3 ~ LC13 are load cases with combined turbulent wind and irregular waves. In LC6, the significant wave height and peak period are correlated with the wind condition at the North Sea Center site (Li et al., 2015). The wind turbulence intensity is calculated according to the IEC class A, which is the design class for the DTU 10 MW wind turbine (Bak et al., 2013). The wind and wave parameters are varied around LC6 to study the impacts of different factors on the system dynamic motion response, including wind and wave directions (aligned and misaligned), significant wave height, wave peak period and mean wind speed.

Turbulent winds are used in all load cases. The TurbSim (Jonkman, 2009) is used to generate the three dimensional turbulent wind field according to the Kaimal turbulence model. The irregular waves are long crested and are modeled by using the JONSWAP spectrum.

For each load case, the simulation lasts for 1 h after removing the start-up transients. The statistical values and power spectra of the dynamic motion response are obtained based on the 1 h simulation results.

7. Results and discussion

The results from the time domain simulations are discussed in this section. The characteristics of the vessel motion (6 DOFs), the crane tip movement (3 DOFs), the blade motion at its COG and the corresponding translational motion at the blade root (3 DOFs) are investigated. The blade root is considered as a point on the blade which is modeled as a rigid body. Therefore, the translational motion of the blade root are obtained from the 6 DOF rigid-body motion of the blade. Tensions in the boom wires, lift wire, slings and tugger lines are not discussed here due to their marginal fluctuations.

7.1. Motion of the vessel

The vessel motion is defined in the vessel-related coordinate system in Fig. 9. Fig. 12(a) show the standard deviations of the vessel translational motion in LC1 ~ LC13 while those in Fig. 12(b) present those of the vessel rotational motion. The vessel motion is zero in LC1 as it is fixed during the numerical simulation. The vessel heave motion is negligible.

Comparisons between LC2 and LC3~LC13 reveal that the wave-induced motion of the vessel dominates over the wind-induced response. The wind loads are further shown to have minor influence on the vessel

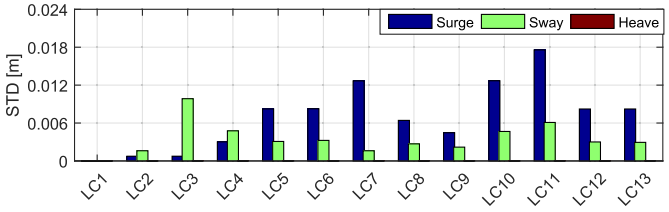

(a) Translational motion

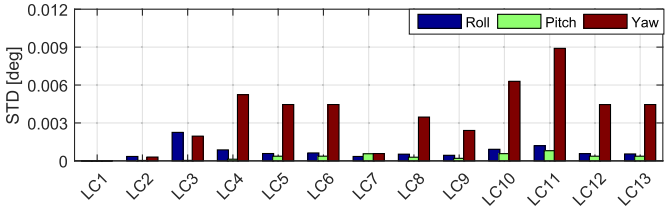

(b) Rotational motion

Fig. 12. Standard deviations of the vessel motion in the vessel-related coordinate system defined in Fig. 9.

motion, compared to the wave load, by comparing LC5 and LC6, and LC6, LC12 and LC13. The vessel motion is sensitive to the incident wave direction, as shown by comparing the results in LC3, LC6 and LC7. It is also dependent on the wave height, which can be observed in the results for LC6, LC8 and LC9. The vessel motion is marginally affected by the cancellation and enhancement effects in wave loads, as shown by the results in LC10 and LC11. The amplitudes of vessel motion show a increasing trend with decreasing wave peak period.

The vessel motion spectra are analyzed. Fig. 13 shows the spectra of vessel motion in surge, sway and yaw. The spectra of vessel pitch and roll motion are similar to those of surge and sway motion, respectively. The power spectrum of vessel surge motion is dominated by the surge resonant response. The vessel sway motion is dominated by the vessel sway resonant response in LC3 ($\theta_{wv} = 0^o$) while notable contributions from the crane resonance response are observed in LC6 and LC11 ($\theta_{wv} = 65.87^o$). The vessel yaw motion is mainly dominated by the vessel yaw resonant response.

7.2. Motion at the crane tip

The crane tip motion is important for crane operations at a large lifting height. The characteristics of the crane tip motion are discussed in this section. The standard deviations of crane tip motion in the vessel related-coordinate system are presented in Fig. 14.

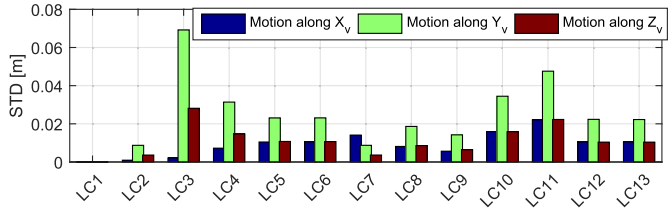

Fig. 14. Standard deviations of the crane tip motion in the vessel-related coordinate system defined in Fig. 9.

Both the vessel motion and the crane deformation contribute to the crane tip motion. The crane deformation includes the deformation of the boom wires and the crane boom, while the deformation of the latter is much marginal compared to that of the former. The crane is deployed in the vertical $O_vY_vZ_v$ plane during the operation, as shown in Fig. 9. As a result, the crane tip motion along X_v and Z_v gets significant contributions from the crane resonant response due to crane deformation, as can be observed in their power spectra shown in Fig. 15. The crane tip motion along X_v has minor contributions of crane resonant response and is mainly resulted from the vessel motion.

The crane tip motion is marginally affected by the variation of wind conditions, as shown by comparing it's standard deviations in LC5, LC6, LC12 and LC13 in Fig. 14. Similar to the vessel motion, the crane tip motion is sensitive to the wave excitation. The comparisons among the results in LC6, LC10 and LC11, and LC6, LC8 and LC9 show that the crane tip motion decreases significantly with reduction in the significant wave height and wave peak period.

7.3. Motion of the installed blade

The 6 DOF rigid-body motions of the blade, with the reference point at its COG, are studied in this section. The motions are defined in the blade-related coordinate system in Fig. 11. The first 3 DOF motions refer to the translational motions at the COG while the rest 3 DOF motions refer to the rotational motions around the COG. Their standard deviations in LC1~13 are shown in Fig. 16.

It can be observed that the blade roll motion is much larger than the blade yaw motion in Fig. 16(b), since the latter is well controlled by the tugger lines deployed perpendicular to the blade span while the former experiences limited restoring force from the tugger lines.

Comparisons among LC1~3 show that the blade surge, heave and pitch motions experience significant contributions from the vessel motion and crane movement. They show large dependency on the wave condition (LC3, LC6 ~LC11) and are marginally affected by the wind properties (LC5, LC6, LC12 and LC13). They are dominated by a combination of the crane resonant response and the vessel sway resonant motion, as shown by the power spectra of blade surge motion in Fig. 17.

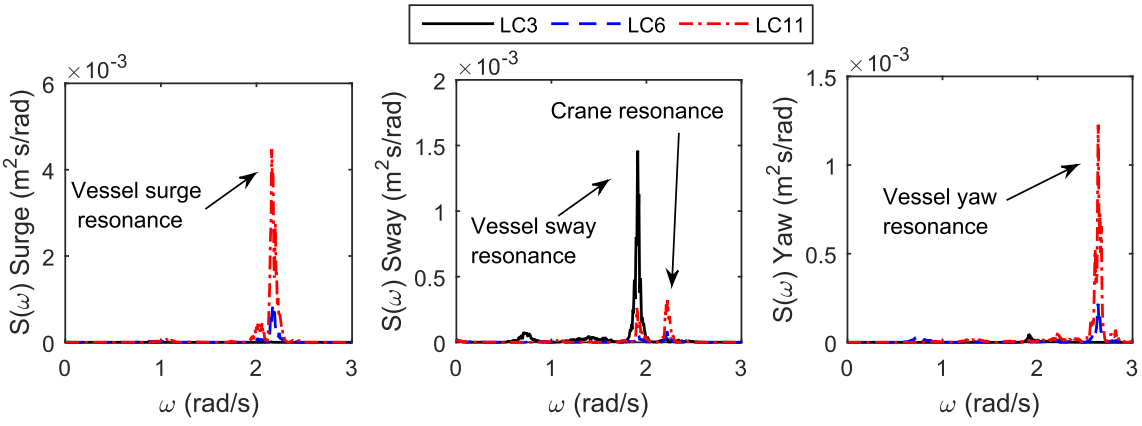

Fig. 13. Power spectra of surge, sway and yaw motion of the vessel in LC3, LC6 and LC11 in the vessel-related coordinate system in Fig. 9.

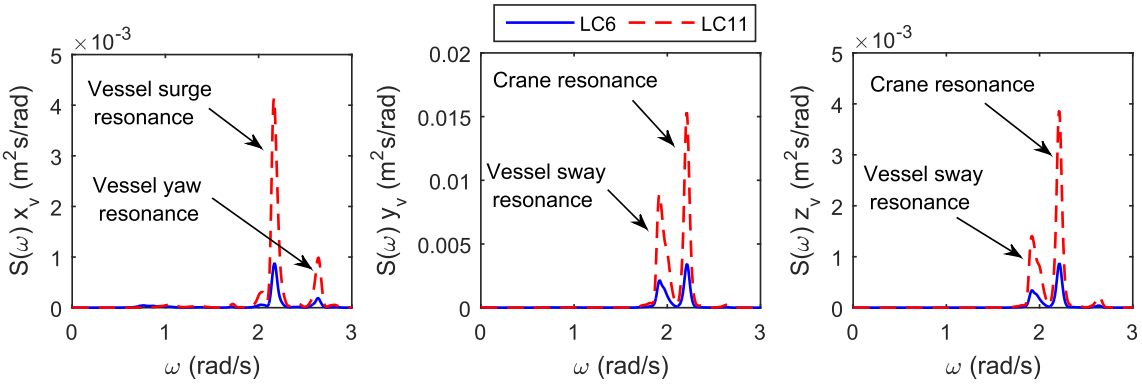

Fig. 15. Power spectra of the crane tip motion in LC6 and LC11: from left to right-along X_v, Y_v and Z_v in the vessel-related coordinate system shown in Fig. 9.

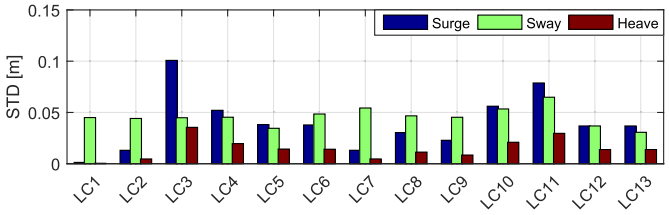

(a) Translational motion

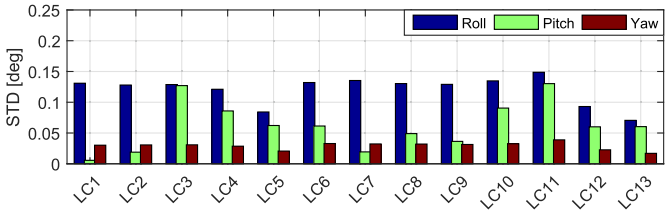

(b) Rotational motion

Fig. 16. Standard deviations of the blade motion in the blade-related coordinate system defined in Fig. 11.

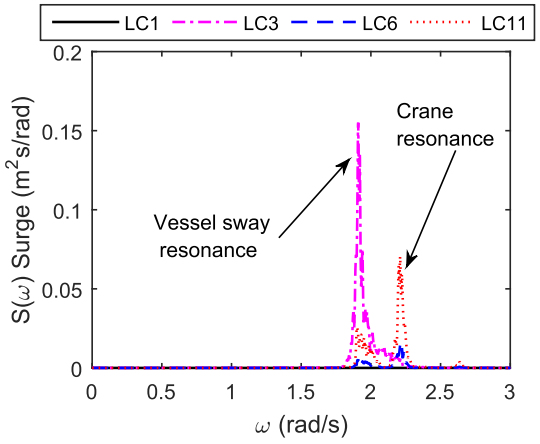

Fig. 17. Power spectra of blade surge motion in LC1, LC3, LC6 and LC11.

The dominance of these two contributions is dependent on the wave direction.

The blade motion in sway, roll and yaw is mainly induced by blade aerodynamic load. The power spectra of blade sway and yaw motions are presented in Fig. 18. The blade sway motion is completely dominated by the blade roll resonant response in LC1. Consideration the vessel and crane motion introduces another two peaks into its power spectrum, due to the double pendulum induced response and the vessel surge resonant motion, as shown in Fig. 18(a). These two peaks are negligible in the spectrum of blade yaw motion in Fig. 18(b). The blade yaw motion is dominated by the blade roll and yaw resonant responses. Consideration the vessel and crane motion increases the contribution from the blade yaw resonant motion. The effects of the vessel and crane motion on blade motion in sway, roll and yaw are significant in short waves.

7.4. Motion at the blade root

The blade root motion is critical during the final mating phase of blade installation. The mating process is not possible if the blade root motion is too large. The characteristics of the translational motion at blade root in the blade related coordinate system in Fig. 11 are studied in this section.

Fig. 19 shows the standard deviations of the blade root motion. Comparing results in LC1~LC3 indicates that the blade root motion would be significantly underestimated, especially along X_b, if the detailed modeling of vessel and crane motion is not considered. Larger underestimation is expected to occur in shorter waves, as indicated by comparing the power spectra of blade root motion in LC1, LC6 and LC11 in Fig. 20.

The displacements of blade root in the global coordinate system are further compared with those of the vessel origin, the crane tip and the blade COG, as shown in Table 10. The blade root motion along Y is mainly resulted from that of the blade COG. The blade root motion along Z is much larger than that of the blade COG, due to the notable contribution from blade roll motion. In LC3~11, the blade root motion along X is close to that of blade COG because the contribution from blade yaw motion becomes relatively less important. The displacements of the blade root and blade COG are much larger than those of the crane tip and the vessel origin. Detailed system modeling including the blade, the vessel and the crane is recommended for numerical analysis of offshore wind turbine blade installation.

8. Conclusions

This study deals with the development, evaluation and application of a fully integrated simulation tool, namely SIMO-RIFLEX-Aero, for modeling and dynamic response analysis of single blade installation for offshore wind turbines using a jack-up crane vessel. The developed simulation tool can account for aerodynamics, hydrodynamics, soil and structural dynamics and wire coupling mechanics.

A coupled SIMO-RIFLEX model for a typical elevated jack-up crane vessel is first developed, considering wave loads on the vessel legs, wind loads on the vessel, structural flexibility of the legs and the crane, soil-structure interaction, as well as important non-linear effects, such as P–Δ effect and leg inclination. Eigen value analysis is conducted to

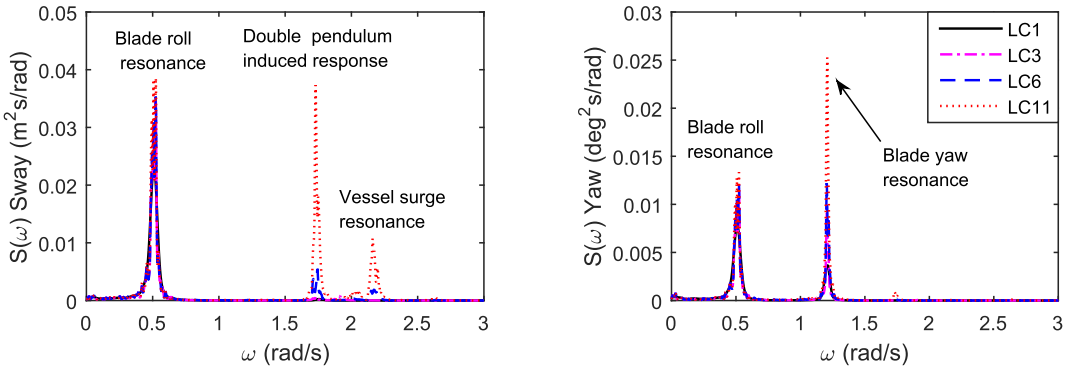

(a) Sway (b) Yaw

Fig. 18. Power spectra of blade sway and yaw motion in LC1, LC6, LC11 and LC13.

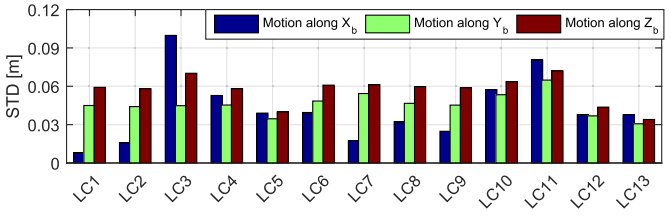

Fig. 19. Standard deviations of the blade motion along X_b, Y_b and Z_b in the blade-related coordinate system defined in Fig. 9.

analyze the eigen periods and mode shapes of the vessel motion. The natural periods of the vessel motion are found to be in the order of 0.4–3s, which are lower than typical wave periods. However, the vessel motion resonances in the longitudinal, transverse and torsional degrees can still be excited, especially in short waves. The first two longest periods are compared with values estimated by empirical formula recommended by standards and guidelines. The developed SIMO-RIFLEX model is then coupled with the SIMO-Aero code (Zhao et al., 2018) to achieve the integrated simulation tool SIMO-RIFLEX-Aero.

The fully coupled SIMO-RIFLEX-Aero code is then applied to simulate the dynamic response of the DTU 10 MW wind turbine blade being installed by a jack-up crane vessel under different stochastic wave and wind conditions in time domain. The vessel motion is mainly induced by wave loads on the jack-up legs. A decrease in wave period and an increase in wave height can cause significant increase in the vessel motion. The vessel motion is dominated by the vessel's surge, sway and yaw resonant response with contribution from the crane's resonant response. Significant crane tip motion is induced by the vessel motion, together with the crane flexibility. The crane tip motion in sway and heave is dominated by the crane resonant response.

The motion of the installed blade are significantly affected by the crane motion caused by the vessel motion due to wave load on the legs. Crane tip motion contributes to much larger blade motion in surge, heave and pitch. Increases in the blade sway, roll and yaw motion are also caused by the crane tip motion in short waves while in long waves they are not. As a result, the blade root motion is significantly increased both along and normal to the hub axis. The blade root velocity is expected to experience larger increase in short waves, which can lead to high potential of damaged guide pins during the final connection phase.

It is essential to plan offshore operations by using an integrated numerical model and analysis. It is revealed in this study by taking the offshore wind turbine blade installation using a jack-up crane vessel as an example. In addition to the direct modeling of the blade motion under wind loads, modeling of the jack-up vessel and the crane is also of great importance for a more safe and efficient installation operation. The vessel motion can cause significant motion at the crane tip during lifting operations at large heights. The crane tip motion due to the vessel motion and crane flexibility can also greatly increase the motion of the lifted components, and hence affects the safety and efficiency of the operation.

The methodology developed in this study can also be applied to deal with other types of offshore lifting operations using jack-up crane vessels.

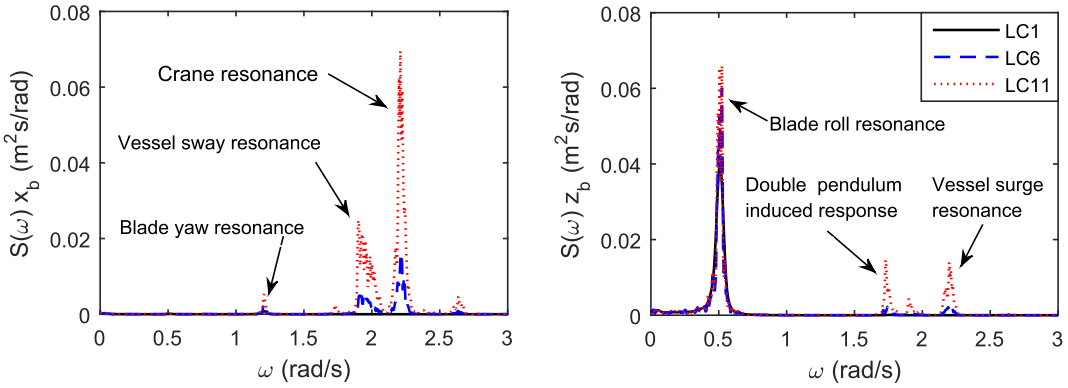

(a) Motion along X_b (b) Motion along Z_b

Fig. 20. Power spectra of blade root motion along X_b and Z_b in LC1, LC6 and LC11 in the blade-related coordinate system defined in Fig. 9.

Table 10
Comparison of displacement variations for the vessel origin (V), crane tip (C), blade (B) and blade root (BR) in the global coordinate system shown in Fig. 9.

	σ_X [cm]				σ_Y [cm]				σ_Z [cm]			
	V	C	B	BR	V	C	B	BR	V	C	B	BR
LC1	–	–	0.13	0.82	–	–	4.50	4.50	–	–	0.05	5.92
LC3	0.99	6.92	10.08	9.98	0.08	0.21	4.49	4.48	0.00	2.82	3.55	7.02
LC6	0.33	2.31	3.78	3.95	0.83	1.05	4.85	4.85	0.00	1.07	1.42	6.09
LC9	0.22	1.42	2.29	2.48	0.45	0.57	4.53	4.53	0.00	0.64	0.85	5.88
LC11	0.61	4.76	7.88	8.06	1.76	2.21	6.49	6.48	0.00	2.23	2.96	7.20

Acknowledgment

The authors appreciate the support from the Department of Marine Technology, Centre for Ships and Ocean Structures (CeSOS) and Centre for Autonomous Marine Operations and Systems (AMOS), NTNU. Thanks are also extended to Mr. Petter Faye Søyland in Fred Olsen Windcarrier for valuable discussions. The first author is financilly supported by the China Scholarship Council (CSC).

References

A2SEA, 2017. Sea installer - offshore wind turbine installation vessel. https://www.a2sea.com/fleet/sea-installer/ (Accessed on 12/24/2017).
Ahn, D., Shin, S.-C., Kim, S.-Y., Kharoufi, H., Kim, H.-C., 2017. Comparative evaluation of different offshore wind turbine installation vessels for Korean west–south wind farm. International Journal of Naval Architecture and Ocean Engineering 9 (1), 45–54.
Bak, C., Zahle, F., Bitsche, R., Kim, T., Yde, A., Henriksen, L.C., Hansen, M.H., Natarajan, A., 2013. Description of the DTU 10 MW Reference Wind Turbine. Tech. Rep. DTU Wind Energy Report-I-0092. Technical University of Denmark.
Carbon Brief Ltd, 2017. Installation of offshore floating wind turbines. https://www.carbonbrief.org/qa-how-viable-are-floating-offshore-windfarms (Accessed on 02/08/2018).
DNVGL, 2015. Recommended Practice DNVGL-rp-c104: Self-elevating Units. Standard. DNVGL, Olso, Norway.
Duan, V., Olsson, F., 2014. Impact Loads on a Self-elevating Unit during Jacking Operation. Master thesis. Chalmers University of Technology.
Fred. Olsen Windcarrier AS, 2016. Specifications for Jack-up Installation Vessels Brave Tern and Bold Tern. Report, Fred. Olsen Windcarrier AS.
Fred. Olsen Windcarrier AS, 2017. Jack-up crane vessels for installation of offshore wind turbines. http://windcarrier.com/fleet/ (Accessed on 02/08/2018).
Friede & Goldman Ltd, 2017. Jack up products: rack chock. http://www.fng.com/engineered-products/jack-up-products (Accessed on 12/24/2017).
Global Data, 2014. Offshore Vessel and Cables Market- Market Size, Competitive Landscape and Key Country Analysis to 2020. Report GDAE1095MAR. GlobalData UK Ltd.
Global Maritime, 2003. Impact of changes to T&R 5-5A on jack-up system reliability levels. Research Report 037. American Global Maritime, Houston, USA.
ISO, 2009. ISO/DIS 19905-1: Petroleum and Natural Gas Industries- Site-specific Assessment of Mobile Offshore Units- Part 1: Jack-ups. Standard. International Organization for Standardization.
Jonkman, B.J., 2009. Turbsim User's Guide: Version 1.50.
Li, L., Gao, Z., Moan, T., 2015. Joint distribution of environmental condition at five european offshore sites for design of combined wind and wave energy devices. Journal of Offshore Mechanics and Ocean engineering 137 (3).
Martin, C.M., 1994. Physical and Numerical Modelling of Offshore Foundations under Combined Loads. Ph.D. thesis. University of Oxford.
Paterson, J., DÁmico, F., Thies, P., Kurt, E., Harrison, G., 2017. Offshore Wind Installation Vessels–a Comparative Assessment for uk Offshore Rounds 1 and 2. Ocean Engineering.
Rayleigh, L., 1877. Theory of Sound (Two Volumes). Dover Publications, New York.
Ringsberg, J.W., Daun, V., Olsson, F., 2017. Analysis of impact loads on a self-elevating unit during jacking operation. J. Offshore Mech. Arctic Eng. 139 (3) 031602.
Scaldis Salvage and Marine Contractors NV, 2018. Single lift of fully assembled offshore wind turbine tower installation. http://www.scaldis-smc.com/en-GB/rambiz-3000/31 (Accessed on 02/08/2018).
SINTEF Ocean, 2017a. RIFLEX 4.10.1 Theory Manual.
SINTEF Ocean, 2017b. Simo-theory Manual Version 4.10.
SNAME, 2008. Technical & Research Bulletin 5-5A: Guidelines for Site Specific Assessment of Mobile Jack-Up Units.
Van Dalfsen, A., 2016. Integral Soil-jack-up Modelling-modelling Site-specific Jack-up Response and Performing Safety Assessment. Master thesis. Delft University of Technology.
Zeng, J., Yuan, H., Wang, C., Wang, Y., Mo, J., 2015. The research on the fatigue analysis of the jack-ups leg based on sesam software. In: ASME 2015 34th International Conference on Ocean, Offshore and Arctic Engineering, May 31-June 5, 2015, St. John's, Newfoundland, Canada. American Society of Mechanical Engineers, V007T06A068–V007T06A068.
Zhao, Y., Cheng, Z., Sandvik, P.C., Gao, Z., Moan, T., 2018. An integrated dynamic analysis method for simulating installation of a single blade for offshore wind turbines. Ocean Eng. 152, 72–88.